Pyrolytic formation of a carbonaceous solid for heavy metal adsorption

A. B. Bourlinos · M. A. Karakassides · P. Stathi ·
Y. Deligiannakis · R. Zboril · P. Dallas ·
T. A. Steriotis · A. K. Stubos · C. Trapalis

Abstract The solid-state pyrolysis of acetylenedicarboxylic acid, monopotassium salt at 300 °C in air results in bulk quantities of a micron-sized yet macroporous oxidized carbon, which inherently possesses high content of metal-binding sites, such as carboxylate groups, free radicals, and ether/hydroxyl units. Besides its high oxygen content, the solid is stable in water and does not leach or disorient, while it also exhibits an appreciable thermal stability, at temperature exceeding 200 °C in air. Several techniques including TEM/SEM, TGA, Raman/FT-IR, XPS, EPR, and potentiometric titrations were employed for the characterization of the solid. Furthermore, liquid phase adsorption experiments revealed that the material is an efficient heavy metal adsorbent due to the presence of diverse surface-accessible binding sites, showing unusually high metal uptake capacities for Pb^{2+} and Cu^{2+} ions (ca. 4.5 mmol g^{-1}).

A. B. Bourlinos (✉) · P. Dallas · C. Trapalis
Institute of Materials Science, NCSR "Demokritos",
Ag. Paraskevi Attikis, 15310 Athens, Greece
e-mail: bourlinos@ims.demokritos.gr

M. A. Karakassides
Department of Materials Science and Engineering,
University of Ioannina, 45110 Ioannina, Greece

P. Stathi · Y. Deligiannakis
Laboratory of Physical Chemistry,
Department of Environmental and Natural Resources
Management, University of Ioannina, Seferi 2,
30100 Agrinio, Greece

R. Zboril
Department of Physical Chemistry, Palacky University,
Svobody 26, 77146 Olomouc, Czech Republic

T. A. Steriotis
Institute of Physical Chemistry, NCSR "Demokritos",
Ag. Paraskevi Attikis, 15310 Athens, Greece

A. K. Stubos
Environmental Research Laboratory, Institute of Nuclear
Technology and Radiation Protection, NCSR "Demokritos",
Ag. Paraskevi Attikis, 15310 Athens, Greece

Introduction

Carbonaceous solids bearing oxygen-containing surface groups (e.g., natural coals) is an interesting class of materials with wide environmental applications such as water softening or purification (i.e., removal of metal ions) [1–7]. These materials are often considered advantageous since they are cheap, adequately stable, and environmentally benign. Nevertheless, their metal-binding capacities are generally low (0.5–1 mmol g^{-1}) compared, for instance, with ion-exchange resin beads (2–5 mmol g^{-1}), and thus, chemical activation is required to increase their capacities. Such activation processes can indeed increase their capacities to values as high as 4 mmol g^{-1}, but eventually result in carbonaceous matrices that leach in aqueous environment, causing thus adverse effects during purification processes [1]. In this respect, the search for new yet simply derived synthetic materials combining high metal-binding capacities with non-leaching properties should be considered as an effort worth trying.

On the other hand, solid-state pyrolysis of suitable organic precursors in air under mild conditions provides a facile, versatile, and, moreover, easily scalable route to directly synthesize a wide range of oxygen-rich carbonaceous materials with interesting physico-chemical properties. This humble approach does not require any advanced experimental setup or delicate reaction conditions except for a persistent searching among a library of organic

compounds to focus on a few promising precursors. In addition, the method leads to single-phase and high-purity materials at yields that are sufficient enough for the preparation of bulk quantities. Finally, such routes allow for direct synthesis of functionalized materials, since some of the chemical properties of the precursor (e.g., heteroatoms, functional groups, carbon hybridization, etc.) are to a large extent retained after mild pyrolysis. Thus, direct incorporation of active sites in the solid is carried out during synthesis without the need of any chemical post-treatment. Following such simple pyrolytic approaches, we have previously demonstrated the formation of a versatile class of carbonaceous materials with peculiar properties, such as thin films [8], porous foams [9], nanoparticles [10, 11], graphite oxide-mimicking layered solids [12, 13], nanosheets [14] as well beads and wires [15].

Along these lines, herein we report a novel carbonaceous solid derived by the mild solid-state pyrolysis (in air) of acetylenedicarboxylic acid, monopotassium salt. Apart from the fact that acetylene is a widely used carbon source (e.g., carbon nanotubes synthesis) this elegant bi-functional molecule provides certain advantages as a precursor since the amount of carboxylic groups (some of which can be retained after pyrolysis) per carbon atom is high. In addition, the small distance between neighboring alkynes may enable their solid-state reaction toward the formation of graphitic nanodomains [16, 17]. The as-obtained material is thermally stable up to 200 °C, insoluble in water (or any other solvent), it possesses a highly developed structure of macropores on the surface, and exhibits an unusually high metal-binding capacity (ca. 4.5 mmol g^{-1}) based on carboxylate groups, free radicals, and ether/hydroxyl units, to name a few. Among other possible applications of these types of materials, in this study, we discuss its use as adsorbent for heavy metals' (e.g., Pb^{2+}, Cu^{2+}) removal from aqueous solutions.

Experimental

Synthesis and reagents

In a typical procedure, 2 g acetylenedicarboxylic acid, monopotassium salt fine powder (Alfa Aesar) was loaded in a small round-bottom porcelain crucible (height: 2 cm; rim diameter: 5 cm) and directly calcined in air at 300 °C for 2 h at a heating rate of 10 °C min^{-1}, using a programmed Carbolite CWF 1100 chamber furnace. Pyrolysis of the salt results in complete expansion to a voluminous but continuous lightweight carbon mass that macroscopically resembles the shape (cylindrical and long tailed) of the classical pharaoh's snake. The diameter of the cylindrical tail was about the size of the crucible nest, whereas

its length was 15–20 cm. As most of the expanded material lay outside the crucible thus contacting the furnace's surroundings, the solid collected for characterization represented the fraction of the carbon tail closest to the crucible. The crude material, which is essentially an admixture of carbon and water-soluble inorganic/organic byproducts, was subjected to repeating washing/centrifugation cycles to obtain a pure carbon phase. In particular, the solid was washed several times with de-ionized water (9 × 50 mL) each one followed by centrifugation, two times with ethanol (2 × 50 mL) also each one followed by centrifugation, and finally dried in an oven at 80 °C. The product was isolated as an insoluble black, lightweight powder with yields of 30–50 mg (i.e., 2–3% yield). Elemental analysis (wt%) of the sample on dry basis gave C: 50.59; H: 3.21; and O: 30–40 (oxygen is estimated by difference). Complementary to these constituents, compensating inorganic cations (e.g., potassium ions from the starting precursor) are also present in the solid, thus filling up the remaining compositional gap (6–16%). At this point, it should be noted that apart from potassium, XPS measurements evidenced the existence of calcium. As the material is an extremely strong Ca^{2+} sorbent, this may be attributed to sorption of Ca^{2+} which is present in traces in the de-ionized water used for washings.

Characterization techniques

The TEM images were obtained on a JEOL JEM 2010 microscope (LaB6 cathode), whereas SEM images were obtained on a Hitachi SU-6600 microscope. Specific surface area (BET) measurements were carried out with N_2 at 77 K on an Autosorb-1 MP volumetric system (Quantachrome) after out-gassing the sample at 120 °C for 15 h. TGA traces were obtained under air with a Perkin-Elmer Pyris TGA/DTA instrument at a heating rate of 10 °C min^{-1}. The Raman spectra were recorded using a Raman microscope system (Renishaw, System 1000) consisting of an optical microscope (Leica) coupled to a Raman spectrometer. Infrared spectra were taken on KBr pellets with a FT-IR spectrometer of Bruker, Equinox 55/S 123 model. The XPS studies were performed in a Kratos Ultra Spectrometer at a base pressure of 1 × 10^{-9} Torr using monochromated Al Kα X-ray source at 1486.6 eV. Electron Paramagnetic Resonance (EPR) spectra were recorded with a Brucker ER200D spectrometer at liquid nitrogen temperatures, equipped with an Agilent 5310A frequency counter. Adequate signal-to-noise was obtained after 5–10 scans. Progressive saturation analysis was performed as analyzed previously [18]. Spin quantization was done using DPPH as spin standard [19]. Numerical simulation of the experimental EPR spectra was performed based on second-order

perturbation theory, using the software WinEPR Simfonia v. 1.25 by Bruker Analytische.

Potentiometric titrations

12.5 mg of material was suspended in a titration cell (Metrohm) containing 12.5 mL of Milli-Q water to yield a concentration of 1 g L^{-1}. The suspension was purged with 99.999% N_2 gas for 30 min before titration. The suspension was then titrated with 12.5 mM NaOH solution using an automatic Metrohm 794 Basic Titrino.

The experimental data were fitted with a theoretical titration curve after assuming that H-binding sites are related to carboxylate groups. For this procedure, the number of H-binding sites and the respective acid dissociation constants, pK_a, were the fitting parameters, while the best fit was achieved by three types of carboxyl groups with pK_a = 3.00, 3.80, and 4.60.

Sorption of heavy metal ions

The Pb^{2+} and Cu^{2+} uptake efficiencies of the material were investigated by means of batch aqueous-phase adsorption experiments under different pH values. For a typical experiment, 10 mg of material was suspended in 10 mL aqueous solution of Pb^{2+} or Cu^{2+} (1.5, 3.0, or 4.5 mM) while the pH was adjusted to the desired value (4–8) with variable amounts of HNO_3 or NaOH taken from 100 mM stock solutions. The samples were allowed to equilibrate at room temperature for 120 min under stirring (screening kinetic experiments revealed that equilibrium was attained within 90 min); in all the cases, a negligible pH drift (<0.2) occurred during equilibration. After the completion of equilibration, the suspension was centrifuged, and the metal concentration of the supernatant solution was determined using Anodic Stripping Voltammetry (ASV) with a polarograph (Trace Master5-MD150, Radiometer Analytica), as detailed in reference [20]. The detection limits were 0.2 ppb for Cu^{2+} and Pb^{2+}.

Results and discussion

Morphology and macroscopic properties

The pyrolysis of the precursor leads to a voluminous crude mass that after aqueous workup affords an oxygen-rich carbonaceous solid with high carbon content (Fig. 1). SEM and TEM studies (Fig. 2) reveal that the material is amorphous containing irregular shaped, 1–10-μm specimens. The particles have a sponge-like appearance with sub-micrometer to micrometer macropores, which create an appreciable pore volume and allow access to a
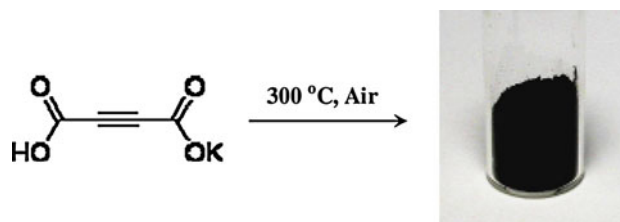
Fig. 1 Solid-state pyrolysis of acetylenedicarboxylic acid, monopotassium salt in air results in bulk quantities of the entitled carbonaceous solid

significant fraction of the matrix [21]. In fact, the solid exhibits a nitrogen BET specific surface area of nearly 17 m^2 g^{-1}, thereby surpassing the literature values for coal substances (1–7 m^2 g^{-1}) [22]. The macroporous structure is likely to originate from the evolution of sizeable CO_2 bubbles during thermal decomposition of the side carboxylate groups of the organic precursor concurrently with the in situ formation of K_2CO_3 crystallites, which are washed away from the carbon matrix after aqueous workup [23, 24].

The material has a strong hydrophilic character; however, it is insoluble in water, forming solid suspensions with no signs of aqueous leaching. Such suspensions can be easily centrifuged or filtered off enabling the collection of clear solutions that do not contain residual debris or contaminants. Furthermore, the material is characterized by a good thermal stability compared with some conventional ion-exchange resins [25, 26]. In particular, TGA measurements under air (Fig. 3) reveal that the thermal decomposition of the solid commences at 220 °C and completes at 450 °C leaving behind a white inorganic residue of carbonate salts. As it is evident from FT-IR measurements (see below) that the material possesses appreciable carboxylate content, these salts presumably result from potassium/calcium carboxylate pending groups after combustion of the carbonaceous matrix.

Vibrational spectroscopy

The Raman profile of the sample is shown in Fig. 4. The spectrum is typical for carbonaceous materials revealing the G and D bands at 1600 and 1380 cm^{-1}, respectively. The width of the peaks (D band is broader than G band) together with the relative intensities ($I_G > I_D$) are consistent with the formation of amorphous carbon [27], i.e., a complex form of carbon containing predominately sp^2 atoms in graphitic nanodomains, as well as, a smaller yet significant sp^3 fraction [21].

Of particular interest are the FT-IR results (Fig. 4). For this study we have examined the spectra of the carbonaceous solid in its de-protonated and protonated form, e.g., –COOK versus –COOH. Note that the carboxylate or

Fig. 2 TEM (*top*) and SEM (*bottom*) images of the carbonaceous solid after aqueous workup. The *inset* SAED pattern is suggestive of amorphous carbon
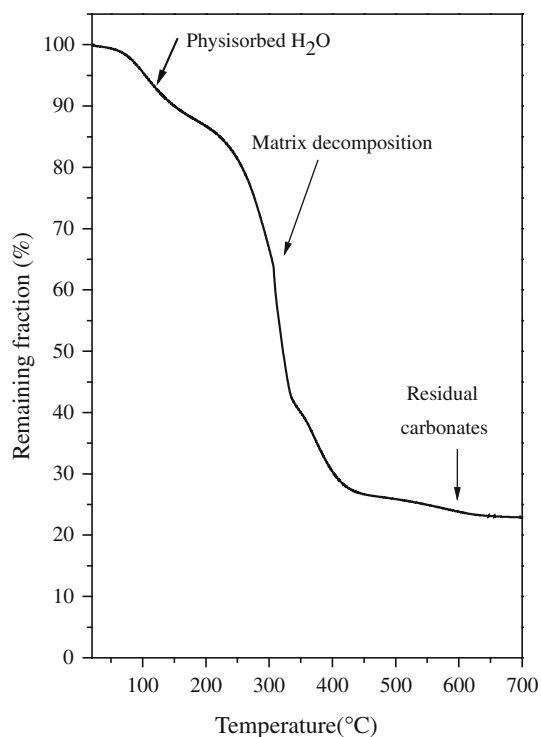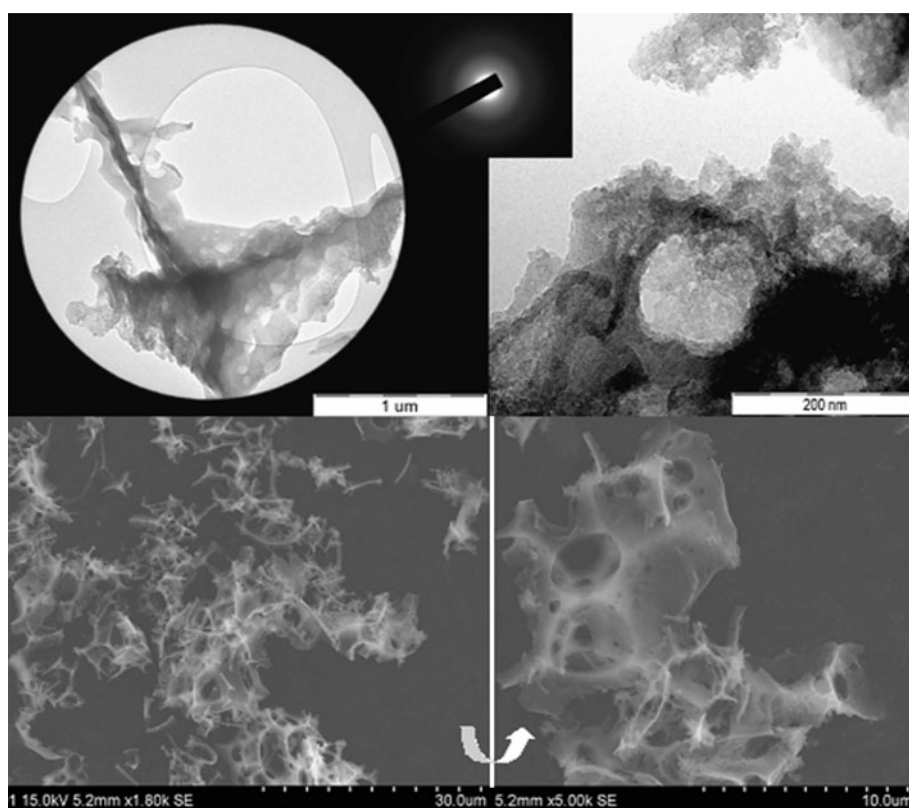

Fig. 3 TGA trace under air of the carbonaceous solid. Residual carbonates were identified by FT-IR spectroscopy

de-protonated form (−COOK) refers to the as-synthesized carbonaceous solid, whereas the protonated form (−COOH) is obtained from the carboxylate one through

aqueous treatment with dilute HCl at pH ∼ 2. With respect to the de-protonated form (−COOK), the spectrum is characterized by three well-defined bands at 1580, 1380, and 600 cm^{-1} as well two other shoulders at 1600 and 1250 cm^{-1}. Accordingly, the intense peaks at 1580 and 1380 cm^{-1} are ascribed to the anti-symmetrical and symmetrical stretching frequencies of −COO^{-} close to benzene rings, respectively [28]. These peaks are the dominant features of the spectrum, thereby suggesting appreciable carboxylate content, which can be attributed to the high carboxylate content of the starting molecular precursor along with the benign pyrolization temperature. On the other hand, the shoulder at 1250 cm^{-1} is due to the C–O stretching vibration in ether/hydroxyl units [29]. In general, basal ether and pending hydroxyl moieties are common functionalities present on the surface of oxidized carbons, particularly those with oxygen-rich content, and result from the thermal oxidation of the precursor in air and thus the reaction of carbon with the atmospheric oxygen. So far, the absorptions at 1580, 1380, and 1250 cm^{-1} merely reflect the different types of surface functionalities present in the carbonaceous solid. Moreover, the remaining bands at 1600 and 600 cm^{-1}, ascribed to vibrations of the carbon lattice, are highly interesting. In detail, the shoulder at 1600 cm^{-1} is associated with the stretching vibration of C=C double bonds (G band) from graphitic nanodomains, whereas the broad absorption at 600 cm^{-1} is also attributed to graphitic sp^2 bonds [30–33]. These normally IR-forbidden vibrations

Fig. 4 *Left*: Raman spectrum of the as-synthesized carbonaceous material (carboxylate or de-protonated form; −COOK). *Right*: comparative FT-IR spectra of the carboxylate (−COOK) and protonated (−COOH) derivatives
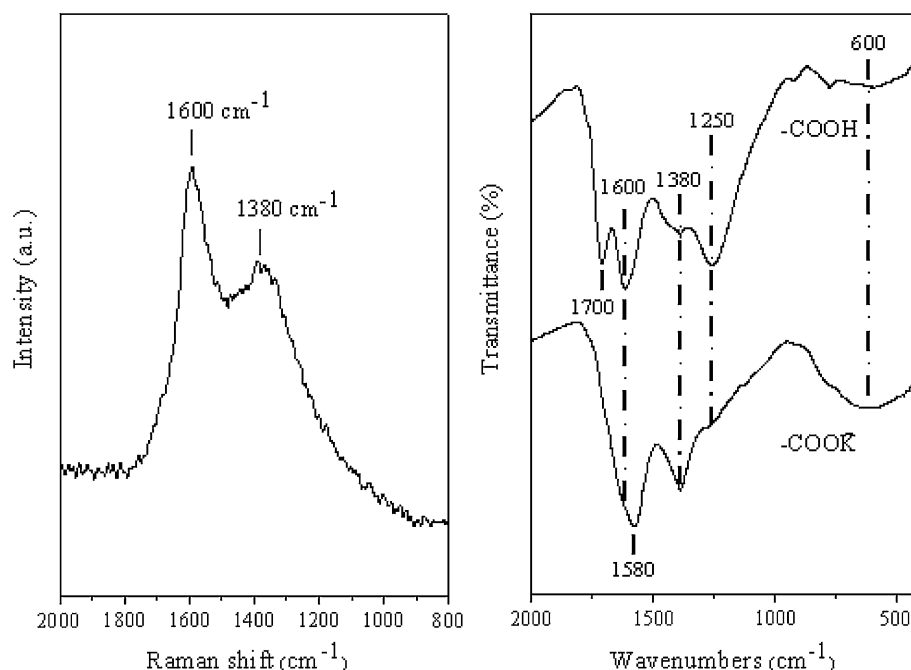
become active when the sp^2 symmetry of the graphitic rings is broken by the insertion of sp^3 carbon atoms as well that of heteroatoms (H and O) in the lattice [30–33]. In other words, the symmetry breaking of graphene allows for the so-called doing Raman with IR. In addition to the G band at 1600 cm^{-1}, one should be also expecting to see the accompanying D band at 1380 cm^{-1} in the FT-IR spectrum. However, this is not possible for the −COO$^-$ form due to the coincidence of this normally weaker band with the stronger symmetrical stretching absorption of the carboxylate unit. Nevertheless, protonation of the carbonaceous solid with dilute HCl (e.g., −COOH) unravels both the G and D bands at 1600 and 1380 cm^{-1}, respectively, with widths and relative intensities remarkably similar to those observed in Raman. Moreover, the sharp symmetrical and anti-symmetrical bands for −COO$^-$ are suppressed after protonation giving rise to a new sharp band at 1700 cm^{-1}, attributable to the carbonyl stretching vibration in −COOH groups. Finally, the band of the ether/hydroxyl groups at 1250 cm^{-1} becomes well defined after protonation, whereas the broad band at 600 cm^{-1} due to graphitic sp^2 bonds is still visible.

XPS spectroscopy

In line with the FT-IR results, XPS spectroscopy was used to investigate the surface functionalities of sample via employing the binding energies of the C 1s and O 1s photoelectrons of the surface groups (Fig. 5). The C 1s pattern splits into two distinct features: a small peak centered at 286 eV that corresponds to carbon bonded to oxygen (e.g., C–O in carboxyl and ether/hydroxyl groups)

and a dominant peak at 282 eV pertaining to carbon–carbon bonds (e.g., graphitized carbon) [33, 34]. On the other hand, the O 1s spectrum shows a peak at 528.5 eV which is typical for oxygen atoms in carboxyl and ether/hydroxyl groups [33, 34].

EPR spectroscopy

The solid-state EPR spectrum of the material is presented in Fig. 6. At 77 K, the EPR spectrum is characterized by a single Gaussian derivative with $\Delta H_{pp} = 3.3$ G and $g = 2.005 \pm 0.001$, while at 300 K, a line narrowing is observed ($\Delta H_{pp} = 3.0$ G) with no g-shift. The calculated spin concentration was 10 μmol g^{-1}, indicating a relatively large population of stable, free radicals, while the Gaussian line-shape implies an inhomogeneous broadening mechanism. The EPR data obtained show that the unpaired spins have restricted mobility on the carbon material. Similar signals have also been recorded for other carbon-based materials, like graphitic nanoparticles, carbon nanofoam, and nanohorns [35–37].

Another important feature is the rather high g-value (2.005), which is considerably higher than the g-values for graphitic nanoparticles ($g = 2.0023$), nanofoam ($g = 2.0029$–2.0032), or nanohorns ($g = 2.0023$) [35–37]. In our case, delocalization of the unpaired spin on O-atoms can justify the up-shift of the g-values, e.g., due to the high spin–orbit coupling of the O-atom. The microwave saturation profile indicates a $P_{1/2}$ value ($P_{1/2} \cong 0.68$ mW at 77 K) which implies a relatively strong coupling of the unpaired spin with lattice phonons, probably *via* the spin–orbit of the O-atoms.

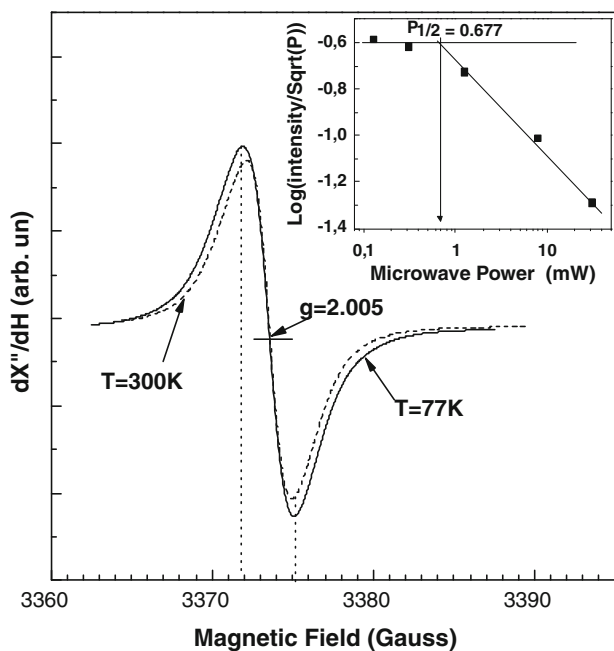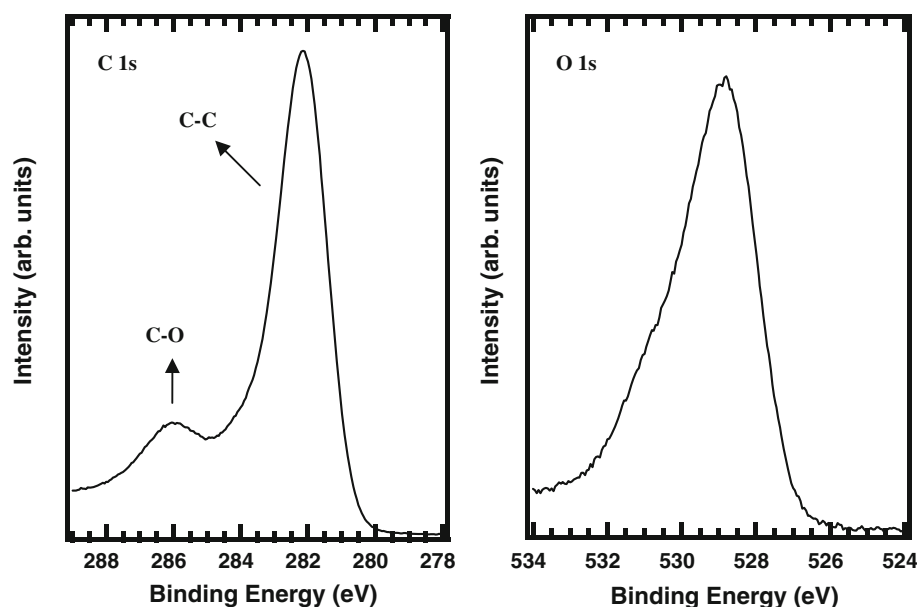**Fig. 5** C 1s and O 1s XPS patterns of the carbonaceous solid

Fig. 6 EPR spectra of the material at 77 K (*solid line*), and 300 K (*dotted line*). *Experimental conditions*: Microwave frequency 9.44 GHz, modulation amplitude 1.00 G, and microwave power 22 dB. *Inset*: Progressive microwave saturation profile at 77 K

H-binding capacity

Potentiometric titrations were used to evaluate the H-binding capacity of the solid. Figure 7a presents the corresponding experimental H-binding data. The solid line in Fig. 7a is a theoretical best-fit, as proposed by the method detailed in [20], assuming three types of carboxyl groups with pK_a = 3.00, 3.80, and 4.60 (close to the pK_a of

acetylenedicarboxylic acid monomer in solution, pK_a = 4.38 [38]). Figure 7b shows the theoretical pH-dependent speciation pattern for the protonable surface groups of the material. As seen from the plot, the major H-binding fraction is due to the carboxyl groups with pK_a = 4.60. Overall, the H-binding data show that the material contains a total of 0.75 ± 0.05 mmol of H-binding carboxylates per gram of material.

Metal uptake

The metal uptake capacity of the material was evaluated for Pb^{2+} and Cu^{2+} ions in pH-dependent adsorption isothermal experiments [20]. Table 1 summarizes the metal uptake results obtained at pH 4, 6, and 8, e.g., values close to the pH of natural or waste waters. In general, adsorption was found to be independent of the pH in the range 4–8, implying that the metal-binding sites behave as permanent charge sites found e.g., in clays [20]. Noteworthy is that the material shows a surprisingly high metal uptake capacity, with a maximum near 4.5 mmol g^{-1} (Table 1). Indeed, the metal uptake is significantly higher than that of montmorillonite clay (0.5–1 mmol g^{-1}), natural coals (0.5–1 mmol g^{-1}), or some synthetic inorganic–organic hybrid materials (<0.1 mmol g^{-1}) [39–41] but quite comparable with that of certain type ion-exchange resin beads (2–5 mmol g^{-1}).

Another interesting result is that the metal adsorbed (mmol g^{-1}) by the material was six times higher than the measured proton uptake (0.75 mmol g^{-1}) and considerably higher than the spin concentration of the solid (10 μmol g^{-1}). It can thus be deduced that carboxylate groups and free radicals can contribute only to a fraction of the metal uptake, while a significant fraction of additional

Fig. 7 a Potentiometric acid–base titration of the material: experimental data (*open square*); theoretical calculation (*solid line*). b Theoretical speciation, derived from the fit of the data in (**a**) using three discrete pK_a values 3.00, 3.80, and 4.60
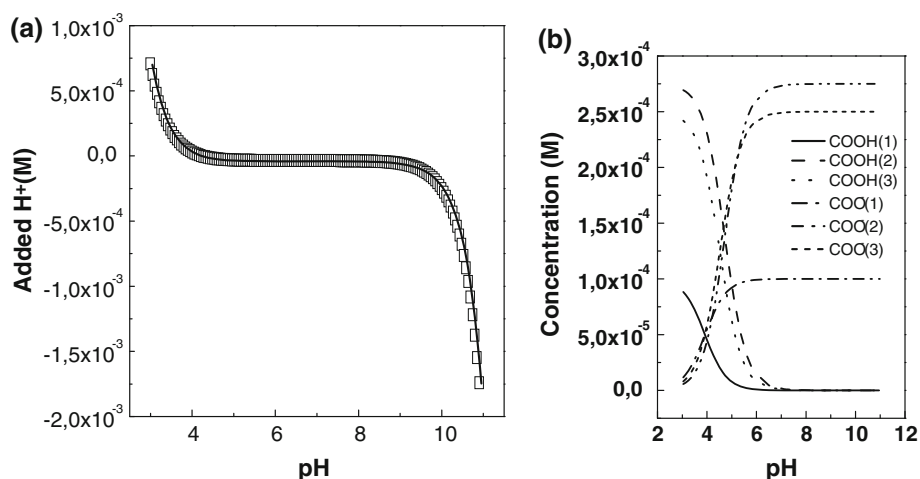

Table 1 Metal uptake results for Cu^{2+} and Pb^{2+} ions obtained at moderate pHs and metal-to-solid ratios

	Cu^{2+} (mmol g^{-1})			Pb^{2+} (mmol g^{-1})	
Initial metal-to-solid ratio	1.5	3.0	4.5	1.5	4.5
pH	Adsorbed metal (mmol g^{-1})				
	Cu^{2+}			Pb^{2+}	
4	1.41	2.85	4.46	1.48	4.47
6	1.49	2.88	4.47	1.49	4.49
8	1.49	2.89	4.47	1.49	4.49

More details are given in the "Experimental" section

strong metal-binding sites are available in the material, for instance, surface ether/hydroxyl groups. These oxygen-bearing units are considered as hard sites that may fix hard metal ions [42, 43]. Accordingly, a given ion may be adsorbed by the ether/hydroxyl groups through the coordinative action of their oxygen's electron lone pairs. Alternatively, residual carbene/carbyne-free edge sites with electron-transfer abilities through metal complexation may also provide additional metal-binding centers. The existence of carbene-like zigzag edge sites and carbyne-like armchair edge sites has been suggested elsewhere [44], and both may originate from the central alkyne group of the precursor. Overall, it appears that the surface of the solid is rather densely covered by several groups that synergically act as strong metal-chelating centers.

In order to further investigate the metal uptake mechanism, we have performed EPR measurements (Fig. 8, solid line) for Cu^{2+} ions adsorbed on the material at pH 8.0. A straightforward observation is that in the Cu^{2+}-treated materials the radical centers were absent, directly demonstrating a strong interaction of Cu^{2+} ions with the radical sites, possibly through partial reduction of Cu^{2+} to Cu^+. The dotted lines of Fig. 8 are the theoretically simulated
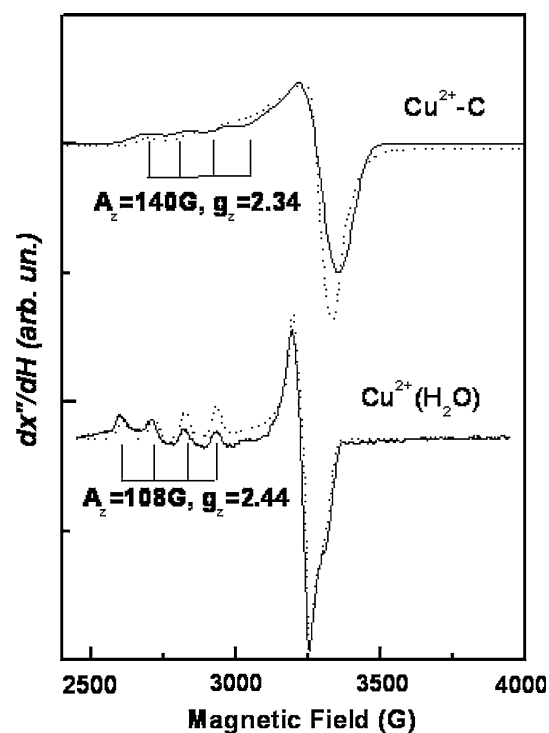

Fig. 8 EPR spectra for the Cu^{2+}-treated material (4.5 mmol g^{-1}, pH 8) and reference $Cu^{2+}(H_2O)$: (*solid lines*) experimental spectra, (*dotted lines*) simulated spectra using the spin Hamiltonian parameters listed in Table 2. *Experimental conditions*: $T = 77$ K, modulation amplitude 10 G, attenuation 10 dB, and Mod. frequency 100 kHz

EPR spectra, calculated as detailed previously [45, 46] after using the spin Hamiltonian parameters listed in Table 2. Analysis of the A_z and g_z values can give detailed quantitative information on the coordination environment of Cu^{2+} ions. In this context, the [A_z vs. g_z] correlation plot offers an appropriate method. By comparing with the literature data [45], the present A_z and g_z values indicate that the bound Cu^{2+} ions are coordinated by at least two oxygen atoms, indicating chelation. Furthermore, the EPR data

Table 2 List of the spin Hamiltonian parameters used for the theoretical EPR simulations

Sample	g_x	g_y	g_z	A_x (G)	A_y (G)	A_z (G)
$Cu^{2+}(H_2O)$	2.059	2.095	2.439	22	13	108
$C–Cu^{2+}$	2.025	2.08	2.34	20	20	140

$Cu^{2+}(H_2O)$ being cited as reference sample, e.g., hydrated Cu^{2+} ions in aqueous solution

show that Cu^{2+} ions are bound in monomeric form, i.e., no clusters are formed even at high pH. This observation further supports the strong chelating power of the functionalized surface.

Summary

In this study, a novel carbonaceous solid with inherently high concentration of surface carboxylate groups, free radicals, and ether/hydroxyl units was synthesized by the solid-state pyrolysis of acetylenedicarboxylic acid, monopotassium salt in air under mild conditions. The carbonaceous matrix has a macroporous structure, it is stable in aqueous solutions, and exhibits a relatively good thermal stability. It is, moreover, characterized by an unusually high metal-binding capacity (ca. 4.5 mmol g^{-1}), which is attributed on the above mentioned active sites. We have demonstrated its potential use as a heavy metal adsorbent, while the material could be further exploited in several separation, purification, and decontamination processes as an alternative to clays, coal substances, or ion-exchange resin beads.

References

1. Lafferty C, Hobday M (1990) Fuel 69:78
2. Sugano M, Mashimo K, Wainai T (1999) Fuel 78:945
3. Wu J, Xu Q, Bai T (2007) Appl Radiat Isot 65:901
4. Pehlivan E, Arslan G (2007) Fuel Process Technol 88:99
5. Sevilla M, Fuertes AB (2009) Carbon 47:2281
6. Demir-Cakan R, Baccile N, Antonietti M, Titirici M-M (2009) Chem Mater 21:484
7. Hu B, Wang K, Wu L, Yu S-H, Antonietti M, Titirici M-M (2010) Adv Mater 22:813
8. Bourlinos AB, Georgakilas V, Zboril R (2008) Carbon 46:1801
9. Bourlinos AB, Steriotis TA, Karakassides M, Sanakis Y, Tzitzios V, Trapalis C, Kouvelos E, Stubos A (2007) Carbon 45:852
10. Bourlinos AB, Stassinopoulos A, Anglos D, Zboril R, Karakassides M, Giannelis EP (2008) Small 4:455
11. Bourlinos AB, Stassinopoulos A, Anglos D, Zboril R, Georgakilas V, Giannelis EP (2008) Chem Mater 20:4539
12. Bourlinos AB, Giannelis EP, Sanakis Y, Bakandritsos A, Karakassides M, Gjoka M, Petridis D (2006) Carbon 44:1906
13. Bourlinos AB, Georgakilas V, Zboril R, Bakandritsos A, Stassinopoulos A, Anglos D, Giannelis EP (2009) Carbon 47:519
14. Bourlinos AB, Steriotis TA, Zboril R, Georgakilas V, Stubos A (2009) J Mater Sci 44:1407. doi:10.1007/s10853-009-3263-8
15. Bakandritsos A, Bourlinos AB, Tzitzios V, Boukos N, Devlin E, Steriotis T, Kouvelos V, Petridis D (2007) Adv Funct Mater 17:1409
16. Skoulika S, Dallas P, Siskos MG, Deligiannakis Y, Michaelides A (2003) Chem Mater 15:4576
17. Dallas P, Bourlinos AB, Komninou P, Karakassides M, Niarchos D (2009) Nanoscale Res Lett 4:1358
18. Stathi P, Louloudi M, Deligiannakis Y (2009) Chem Phys Lett 472:85
19. Chang T (1984) Magn Reson Rev 9:65
20. Stathi P, Litina K, Gournis D, Giannopoulos TS, Deligiannakis Y (2007) J Colloid Interface Sci 316:298
21. Levine DG, Schlosberg RH, Silbernagel BG (1982) Proc Natl Acad Sci USA 79:3365
22. Linge HG (1989) Fuel 68:111
23. Skrabalak SE, Suslick KS (2006) J Am Chem Soc 128:12642
24. Bang JH, Han K, Skrabalak SE, Kim H, Suslick KS (2007) J Phys Chem C 111:10959
25. Petrus L, Stamhuis EJ, Joosten GEH (1981) Ind Eng Chem Prod Res Dev 20:366
26. Raje AP, Datta R (1992) J Mol Catal 72:97
27. Cuesta A, Dhamelincourt P, Laureyns J, Martinez-Alonso A, Tascón JMD (1994) Carbon 32:1523
28. Gasgnier M (2001) J Mater Sci Lett 20:1259
29. Fanning PE, Vannice MA (1993) Carbon 31:721
30. Kaufman JH, Metin S, Saperstein DD (1989) Phys Rev B 39:13053
31. Zhou Z, Xia L (2002) J Phys D Appl Phys 35:1991
32. Ferrari AC, Rodil SE, Robertson J (2003) Phys Rev B 67:155306
33. Zhou J-H, Sui Z-J, Zhu J, Li P, Chen D, Dai Y-C, Yuan W-K (2007) Carbon 45:785
34. Zhang D, Luo H, Wang Y, Feng H (2010) Chem Lett 39:424
35. Lijewski S, Wencka M, Hoffmann SK, Kempinski M (2008) Phys Rev B 77:014304
36. Arcon D, Jaglicic Z, Zorko A, Rode AV, Christy AG, Madsen NR, Gamaly EG, Luther-Davies B (2006) Phys Rev B 74:014438
37. Garaj S, Thien-Nga L, Gaal R, Forro L, Takahashi K, Kokai F, Yudasaka M, Iijima S (2000) Phys Rev B 62:17115
38. Schwartz LM, Gelb RI, Laufer DA (1980) J Chem Eng Data 25:95
39. Ma T-Y, Zhang X-J, Yuan Z-Y (2009) J Mater Sci 44:6775. doi:10.1007/s10853-009-3576-7
40. Ma T-Y, Lin X-Z, Zhang X-J, Yuan Z-Y (2010) New J Chem 34:1209
41. Ma T-Y, Lin X-Z, Yuan Z-Y (2010) Chem Eur J 16:8487
42. Alfarra A, Frackowiak E, Béguin F (2004) Appl Surf Sci 228:84
43. Montes-Morán MA, Suarez D, Menéndez JA, Fuente E (2004) Carbon 42:1219
44. Radovic LR, Bockrath B (2005) J Am Chem Soc 127:5917
45. Peisach J, Blumberg WE (1974) Arch Biochem Biophys 165:691
46. Grigoropoulou G, Christoforidis KC, Louloudi M, Deligiannakis Y (2007) Langmuir 23:10407